Optics Letters

Manipulating electromagnetic waves in a cavity-waveguide system with nontrivial and trivial modes

Jiong Xu,[1] Xiaofei Zang,[1,*] Xudong Zhan,[1] Kun Liu,[1] and Yiming Zhu[1]

[1]Terahertz Technology Innovation Research Institute and Shanghai Key Lab of Modern Optical System, University of Shanghai for Science and Technology, No. 516 JunGong Road, Shanghai, 200093, China
*Corresponding author: xfzang@usst.edu.cn

Received 8 August 2022; revised 8 September 2022; accepted 12 September 2022; posted 14 September 2022; published 29 September 2022

The coupled cavity-waveguide approach provides a flexible platform to design integrated photonic devices that are widely applied in optical communications and information processing. Topological photonic crystals that can excite the nontrivial edge state (ES) and corner state (CS) have an unprecedented capability to manipulate electromagnetic (EM) waves, leading to a variety of unusual functionalities that are impossible to achieve with conventional cavity-waveguide systems. In this Letter, two-dimensional photonic crystals consisting of an ES waveguide, a CS cavity, and a trivial cavity are proposed as a means to robustly control the transmission characteristics of electromagnetic waves. As a proof-of-principle example, the analog of electromagnetically induced transparency (EIT) that is tolerated in disorders due to the robustness of the CS is numerically demonstrated. In addition, the analog of multi-EIT is also verified by introducing a trivial cavity with two degenerate orthogonal modes. This unique approach for robustly manipulating EM waves may open an avenue to the design of high-performance filters, modulators, and on-chip processors.

https://doi.org/10.1364/OL.472677

Photonic crystals consisting of periodic dielectric structures possess photonic bandgaps which give rise to applications in guiding the transmission of EM waves. By simultaneously integrating a waveguide and a cavity into two-dimensional photonic crystals, one can obtain an on-chip coupled cavity-waveguide system [1], which provides an ultra-compact platform to flexibly control the propagation characteristics of EM waves. A variety of applications based on coupled cavity-waveguide systems have been demonstrated, ranging from all-optical buffers [2,3] to sensors [4,5], filters [6–8], Fano effects [9,10], and electromagnetically induced transparency [11–13], to name a few. However, the aforementioned functionalities and applications realized by a traditional coupled cavity-waveguide system (based on photonic crystal) are fragile and easily affected by disorders due to fabrication errors.

Photonic topological insulators (PTIs), in which the ES and CS can be excited due to symmetric protection, have provided an unprecedented capability to manipulate EM waves, and thus a variety of unusual functionalities can be realized [14–20]. In the past few years, a variety of photonic structures to generate ES modes have been proposed and designed [21–28]. Recently, high-order topological insulators (HOTIs) related to CS and hinge states (HSs) have been discovered due to non-zero higher-order multiple moments (i.e., quadrupole and octupole moments) that can be quantized due to crystalline symmetries [29–36]. Unlike a trivial cavity with defect structures [37,38], a topological CS (without defect structures) enables a stronger capability to trap EM waves [39]. By coupling an ES waveguide and CS cavity in a two-dimensionally topological photonic crystal, the unique properties of strong localization and robust transmission lead to unprecedented capabilities to modulate the incident EM waves. However, previous studies [40,41] have mainly focused on the manipulation of EM waves in an ES waveguide coupled with only one trivial or nontrivial cavity. The modulation of EM waves in an ES waveguide coupled with two cavities, i.e., a nontrivial cavity coupled with a trivial cavity, has not attracted much attention, because the constructive and destructive coherence between nontrivial and trivial cavities/modes provides a new degree of freedom to manipulate EM waves.

In this Letter, we propose a coupled cavity-waveguide system consisting of a topological ES waveguide, a CS cavity, and a trivial cavity to study the propagation characteristic of EM waves. The robust transmission characteristic, i.e., the analog of EIT that is immune to disorders, is numerically demonstrated due to the robustness of the CS. In addition, multi-EIT (with a robust transmission characteristic) is also realized by introducing a trivial cavity with two degenerate orthogonal modes. A theoretical model is also constructed to further analyze the simulated transmission spectra.

Figure 1(a) schematically shows the coupled cavity-waveguide system composed of two-dimensional photonic crystals. The structural parameters are as follows: the lattice constant a of the photonic crystal is 25 mm, while the permittivity of the dielectric rods (i.e., the alumina) ε_d is 9.5 (the background index n_a is 1.0). $d_1 = 5.8$ mm, $d_2 = 4.86$ mm, and $W = 5.414$ mm. The ES waveguide is obtained by combining one photonic crystal (PC1) consisting of periodic unit cells of UC1 [see Fig. 1(a)] and another photonic crystal (PC2) composed of periodic unit cells of UC2 [see Fig. 1(a)]. The Zak phases of the designed photonic crystals (PC1 and PC2) are

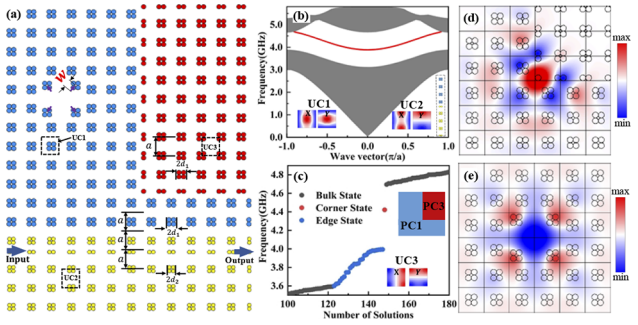

Fig. 1. Schematic and the corresponding resonant modes of the designed cavity-waveguide system. (a) Schematic of the designed system. (b) Projected band of PC1 and PC2; insets show the electric fields (E_z) of UC1 and UC2 at high-symmetry points. (c) Eigenmodes of the combined structure of PC3 and PC1; insets show the electric field (E_z) of UC3 at high-symmetry points. (d) Electric field (E_z) of the topological CS. (e) Electric field (E_z) of the trivial cavity that is far away from the waveguide. Insets in the bottom right corner of (b) and the top right corner of (c) show the models used for the simulations.

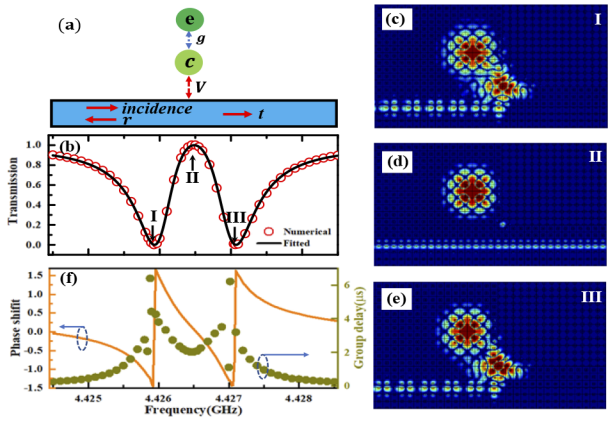

Fig. 2. (a) Theoretical model of the designed cavity-waveguide system. (b) Theoretical (black curve) and calculated (red curve) transmission spectra of the designed cavity-waveguide system. (c), (d), and (e) Calculated electric field ($|E_z|^2$) at points I (4.42592 GHz), II (4.42645 GHz), and III (4.42708 GHz), respectively. (f) Phase shift (yellow curve) and group delay (green curve) of the designed cavity-waveguide system.

quantized and possess values of 0 or π. In fact, the Zak phase of PC1 (or PC2) can be numerically revealed by calculating the electric field (E_z) at high symmetry points in the Brillouin zone [31,42]. When the electric-field distribution at X (Y) (symmetry points in the Brillouin zone) is symmetric or asymmetric, the corresponding Zak phase in the x (y) direction is 0 or π. As shown in the inset of Fig. 1(b), the Zak phases for PC1 and PC2 are (0, 0) and (0, π), respectively. According to the bulk-edge correspondence, there will be edge state(s) in the bandgap of the combined structure (the combination of PC1 and PC2), as shown in Fig. 1(b) (see the red curve). Here, two-way edge states that are not protected by bulks with different topological numbers can be generated (see the detailed discussion in Supporting Materials 1). In contrast, the Zak phase of PC3 (consisting of periodic UC3 at X (Y) points along the x (y) direction) is (π, π) [also see the insets showing the electric-field distributions at X and Y points in Fig. 1(c)]. Therefore, the corner state can be excited by PC3 surrounded by PC1 [see the inset in Fig. 1(c)], and the topological corner charge is determined by the polarization of $Q_c = P_x^{edge} + P_y^{edge} = 1/2 + 1/2 = 1$. The eigenmodes of the hybrid structure composed of PC1 and PC3 are shown in Fig. 1(c), and the topological CS in the bandgap is excited at $f = 4.4214$ GHz. The corresponding electric-field distribution is shown in Fig. 1(d). In addition to the CS cavity, the designed cavity-waveguide system introduces another trivial cavity (in PC1) that can be excited by the CS cavity. The eigenmode (at $f = 4.4201$ GHz) of such a cavity is shown in Fig. 1(e).

The performance of such a cavity-waveguide system [see Fig. 1(a)] is numerically simulated and theoretically analyzed in Fig. 2 (which consists of a waveguide, a CS cavity, and a trivial cavity). The theoretical schematic of our designed cavity-waveguide system [see Fig. 1(a)] is shown in Fig. 2(a). Therefore, the Hamiltonian of the theoretical mode can be described as [43,44]

$$H = \int dx \left[C_R^\dagger(x) \left(\omega_0 - i v_g \frac{\partial}{\partial x} \right) C_R(x) + C_L^\dagger(x) \left(\omega_0 + i v_g \frac{\partial}{\partial x} \right) C_L(x) \right], + \omega_c C_c^\dagger C_c + \omega_e C_e^\dagger C_e + \int dx V \delta(x) [C_R^\dagger(x) C_c + C_L^\dagger(x) C_c] + g C_c^\dagger C_e + h.c, \quad (1)$$

where $C_L(x)$ ($C_R(x)$) is the annihilation operator of the left-moving (right-moving) edge state (ES). v_g is the group velocity of the ES. C_i ($i = c, e$) is the annihilation operator of the i^{th} cavity with a corresponding eigenfrequency of ω_i. $V(g)$ describes the coupling between the cavity C and the waveguide (cavity e). The stationary eigenstate of the Hamiltonian is given by

$$|\Phi\rangle = \int dx [\phi_R(x,t) C_R^\dagger(x) + \phi_L(x,t) C_L^\dagger(x)] |\Theta\rangle + \left(\sum_{i=c}^{e} \phi_i(t) C_i^\dagger \right) |\Theta\rangle, \quad (2)$$

where $\phi_L(x)$ ($\phi_R(x)$) and ϕ_i are the wave functions of the left-moving (right-moving) ES in the waveguide and cavities, respectively. $|\Theta\rangle$ is the vacuum state. The transmission coefficient (t) can be deduced from $H|\Phi\rangle = i\hbar \frac{\partial}{\partial t} |\Phi\rangle$:

$$t = \frac{(\omega - \omega_e)(\omega - \omega_c) - g^2}{(\omega - \omega_e)(\omega - \omega_c + i\frac{V^2}{V_g}) - g^2}. \quad (3)$$

According to Eq. (3), a symmetric transmission spectrum containing one peak and two dips is observed, as shown in Fig. 2(b) (black curve; the fitted parameters and the effects of these parameters are given in Table I of the supporting materials). When $\omega = \Omega = 4.4265$ GHz, the complete transmission of incident EM waves (shown as a peak) is realized, while two side dips at $\omega_{L/R} = \Omega \pm g$ ($\omega_L = 4.4259$ GHz and $\omega_R = 4.4271$ GHz) are related to Rabi splitting. The numerically calculated transmission spectrum is shown in Fig. 2(b) (see the circular curve, which was calculated based on COMSOL), which is well matched with the theoretical mode (the difference between the fitted and simulated spectra is given in Supporting Materials 2). The electric-field intensity distributions at points I, II, and III are shown in Figs. 2(c)–2(e) and demonstrate the EIT-like transmission characteristic. The phase shift and group delay are shown in Fig. 2(f). The group delay at 4.4265 GHz (with $T = |t|^2 = 1$) is about 2 μs.

Although the traditional cavity-waveguide system can realize the EIT-like phenomenon, it is limited to fabrication errors/disorders, which means that the manipulation of EM waves in the traditional cavity-waveguide system is fragile and

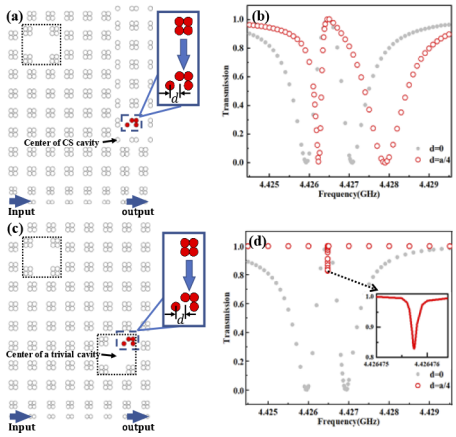

Fig. 3. (a), (c) Schematics of the designed cavity-waveguide system by embedding disorders. The cavity closed to the waveguide can excite a corner state (a) or a trivial mode (c). (b), (d) Transmission spectra (red curves for the calculated results) in the designed systems shown in (a) and (c), respectively. The gray curves in (b) and (d) are the transmission spectra in (a) and (c) without disorders. The dotted black boxes show the trivial cavities.

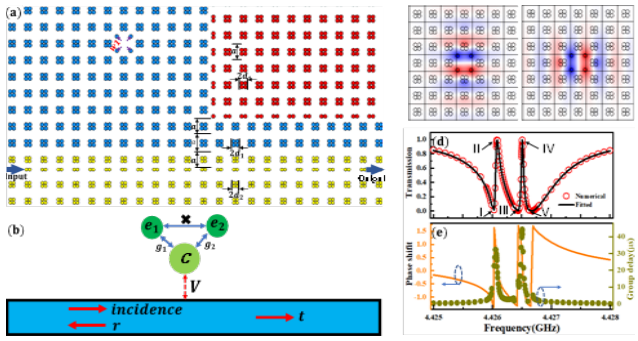

Fig. 4. (a), (b) Schematic and theoretical model of the cavity-waveguide system. (c) Eigenmodes of the trivial cavity that can generate two degenerate and orthogonal resonant modes at 4.4261 GHz. (d) Theoretical (black curve) and calculated (red curve) transmission spectra of the designed cavity-waveguide system. (e) Phase shift (yellow curve) and group delay (green curve) of the designed cavity-waveguide system.

easily affected by disorders. In contrast, our proposed cavity-waveguide system is immune to the disorders resulting from fabrication errors. As a proof-of-concept example, we introduce disorders into the CS cavity and demonstrate the robust transmission characteristic of EM waves. As schematically shown in Fig. 3(a), the disorder is introduced by shifting a rod that is in the diagonal direction of the CS cavity. The calculated transmission spectrum for $d = 6.25$ mm ($= a/4$) is illustrated in Fig. 3(b) (see the red curve). In this case, the calculated detuning between the CS cavity and trivial cavity is about 0.001 GHz, which can be considered to be small detuning (between these two cavities). Therefore, an EIT-like transmission spectrum is also obtained (see the electric-field intensity distributions at the peak and two dips in Supporting Materials 3). In contrast, when the CS cavity is replaced by a trivial cavity (and the EIT-like transmission spectrum appears for $d = 0$; see the dotted gray curve in Fig. 3(d)), and the disorder is introduced by shifting a rod that is in the diagonal direction of the center of the trivial cavity (see Fig. 3(c)), the EIT-like phenomenon disappears from this system (see the red curve in Fig. 3(d), which is due to the independently excited trivial cavity far away from the waveguide). In this situation [for $d = 6.25$ mm ($= a/4$)], the detuning between these two trivial cavities is about 0.0933 GHz, which means that the trivial cavity far from the waveguide cannot be excited by the trivial cavity (close to the waveguide) due to the strong detuning between these two trivial cavities. It should be noted that these two trivial cavities are only independently excited (for $d = 6.25$ mm) without coupling with each other, resulting in the disappearance of the EIT-like phenomenon (detailed discussions of this are shown in Supporting Materials 3). In comparison with Figs. 3(b) and 3(d), we can conclude that the analog of EIT can be maintained (with the disorders) in our designed cavity-waveguide system.

In addition, the proposed device can also manipulate EM waves with multiple EIT-like transmission characteristics by introducing a trivial cavity with two degenerate and orthogonal resonant modes, as shown in Fig. 4(a). The structural parameter for such a trivial cavity is $w_1 = 8$ mm [the other structural parameters are the same as in Fig. 1(a)]. The theoretical schematic of such a designed cavity-waveguide system is shown in Fig. 4(b), and thus the transmission coefficient (t) for the theoretical model [deduced from Fig. 4(b)] is governed by (see the detailed theoretical model in Supporting Materials 4)

$$t = \frac{(\omega-\omega_{e1})(\omega-\omega_{e2})(\omega-\omega_c)-(\omega-\omega_{e2})g_1{}^2-(\omega-\omega_{e1})g_2{}^2}{(\omega-\omega_{e1})(\omega-\omega_{e2})(\omega-\omega_c+i\frac{V^2}{V_g})-(\omega-\omega_{e2})g_1{}^2-(\omega-\omega_{e1})g_2{}^2}. \quad (4)$$

The eigenmodes of the trivial cavity [located at the top left corner; see Fig. 4(a)] are excited at $\omega_{e1} = \omega_{e2} = 4.4261$ GHz, and two degenerate orthogonal modes are generated, as shown in Fig. 4(c). g_1 and g_2 describe the coupling between the CS cavity and the trivial cavity (with two degenerate orthogonal modes). Since these two resonant modes (in the cavity that is far from the waveguide) are asymmetrically distributed to the CS cavity, the resonant frequencies of these two orthogonal modes will be split into two separate frequencies, and thus the constructive coherences between the CS and the two orthogonal resonant modes will generate two transparent peaks in the transmission spectrum [see the fitted and calculated transmission spectra in Fig. 4(d); the fitted parameters and the effects of these parameters are given and discussed in Table II of the supporting materials], leading to the multiple EIT-like transmission characteristic (the difference between the fitted and simulated spectra is given in Supporting Materials 2, and the electric-field intensity distributions at I, II, III, IV, and V are given in Supporting Materials 5). The phase shift and group delay are shown in Fig. 4(e), and the group delay at 4.4261 GHz and 4.4265 GHz (with $T = |t|^2 = 1$) is about 22 μs and 41 μs, respectively. The robust characteristics of this multiple EIT-like phenomenon are discussed in Supporting Materials 6.

In summary, a cavity-waveguide system containing an ES waveguide, a CS cavity, and a trivial cavity was constructed to robustly control the propagation of EM waves. In contrast to conventional cavity-waveguide systems, this work showed that the propagation characteristic of EM waves is robust and immune to disorders. As proof-of-principle examples, robust EIT and multi-EIT were also demonstrated in the designed system. This unique approach for robustly manipulating EM waves

may open a new window to the design of ultra-compact devices with high-performance applications.

Funding. National Key Research and Development Program of China (2017YFA0701005); National Natural Science Foundation of China (61871268, 62271320); "Shuguang" Program of Shanghai Education Commission (19SG44); Shanghai international joint laboratory project (17590750300); 111 Project (D18014).

Acknowledgment. Thanks to Dr. Zhiyuan Fan for helpful discussions and simulations.

Disclosures. The authors declare no conflicts of interest.

Data availability. Data underlying the results presented in this paper are not publicly available at this time but may be obtained from the authors upon reasonable request.

Supplemental document. See Supplement 1 for supporting content.

REFERENCES

1. A. Yariv, Y. Xu, R. K. Lee, and A. Scherer, Opt. Lett. **24**, 711 (1999).
2. J. B. Khurgin, J. Opt. Soc. Am. B **22**, 1062 (2005).
3. T. Baba, Nat. Photonics **2**, 465 (2008).
4. J. Scheuer, J. Opt. Soc. Am. B **33**, 1827 (2016).
5. A. Andueza, J. Perez-Conde, and J. Sevilla, Opt. Express **24**, 18807 (2016).
6. J. Romero-Vivas, D. N. Chigrin, A. V. Lavrinenko, and C. M. S. Torres, Opt. Express **13**, 826 (2005).
7. K. Fasihi and S. Mohammadnejad, Opt. Express **17**, 8983 (2009).
8. Z. W. Cheng, J. H. Zhang, J. J. Dong, and Y. H. Ding, Opt. Lett. **46**, 3873 (2021).
9. J. Lian, S. Sokolov, E. Yuce, S. Combrie, A. De Rossi, and A. P. Mosk, Phys. Rev. A **96**, 033812 (2017).
10. M. H. Rezaei and M. H. Yavari, Appl. Opt. **61**, 3156 (2022).
11. M. F. Yanik, W. Suh, Z. Wang, and S. H. Fan, Phys. Rev. Lett. **93**, 233903 (2004).
12. X. D. Yang, M. B. Yu, D. L. Kwong, and C. W. Wong, Phys. Rev. Lett. **102**, 173902 (2009).
13. S. Kocaman, X. Yang, J. F. McMillan, M. B. Yu, D. L. Kwong, and C. W. Wong, Appl. Phys. Lett. **96**, 221111 (2010).
14. B. Bahari, A. Ndao, F. Vallini, A. El Amili, Y. Fainman, and B. Kante, Science **358**, 636 (2017).
15. M. A. Bandres, S. Wittek, G. Harari, M. Parto, J. H. Ren, M. Segev, D. N. Christodoulides, and M. Khajavikhan, Science **359**, eaar4005 (2018).
16. H. L. He, C. Y. Qiu, L. P. Ye, X. X. Cai, X. Y. Fan, M. Z. Ke, F. Zhang, and Z. Y. Liu, Nature **560**, 61 (2018).
17. W. X. Zhang, X. Xie, H. M. Hao, J. C. Dang, S. Xiao, S. S. Shi, H. Q. Ni, Z. C. Niu, C. Wang, K. J. Jin, X. D. Zhang, and X. L. Xu, Light: Sci. Appl. **9**, 6 (2020).
18. A. Dutt, Q. Lin, L. Q. Yuan, M. Minkov, M. Xiao, and S. H. Fan, Science **367**, 59 (2020).
19. L. C. Yang, G. R. Li, X. M. Gao, and L. Lu, Nat. Photonics **16**, 279 (2022).
20. C. C. Lu, Y. Sun, C. Wang, H. Zhang, W. Zhao, X. Hu, M. Xiao, W. Ding, Y. Liu, and C. T. Chan, Nat. Commun. **13**, 2586 (2022).
21. Z. Wang, Y. D. Chong, J. D. Joannopoulos, and M. Soljacic, Nature **461**, 772 (2009).
22. M. Hafezi, S. Mittal, J. Fan, A. Migdall, and J. M. Taylor, Nat. Photonics **7**, 1001 (2013).
23. Y. H. Yang, Z. Gao, H. R. Xue, L. Zhang, M. J. He, Z. J. Yang, R. Singh, Y. D. Chong, B. L. Zhang, and H. S. Chen, Nature **565**, 622 (2019).
24. X. T. He, E. T. Liang, J. J. Yuan, H. Y. Qiu, X. D. Chen, F. L. Zhao, and J. W. Dong, Nat. Commun. **10**, 9 (2019).
25. L. H. Wu and X. Hu, Phys. Rev. Lett. **114**, 223901 (2015).
26. F. Gao, H. R. Xue, Z. J. Yang, K. F. Lai, Y. Yu, X. Lin, Y. D. Chong, G. Shvets, and B. L. Zhang, Nat. Phys. **14**, 140 (2018).
27. R. Zhou, H. Lin, Y. Liu, X. T. Shi, R. X. Tang, Y. J. Wu, and Z. H. Yu, Phys. Rev. A **104**, L031502 (2021).
28. B. Yan, Y. C. Peng, A. Q. Shi, J. L. Xie, P. Peng, and J. J. Liu, Opt. Lett. **47**, 2044 (2022).
29. W. A. Benalcazar, B. A. Bernevig, and T. L. Hughes, Science **357**, 61 (2017).
30. C. W. Peterson, W. A. Benalcazar, T. L. Hughes, and G. Bahl, Nature **555**, 346 (2018).
31. B. Y. Xie, G. X. Su, H. F. Wang, H. Su, X. P. Shen, P. Zhan, M. H. Lu, Z. L. Wang, and Y. F. Chen, Phys. Rev. Lett. **122**, 233903 (2019).
32. Y. Liu, S. W. Leung, F. F. Li, Z. K. Lin, X. F. Tao, Y. Poo, and J. H. Jiang, Nature **589**, 381 (2021).
33. R. Chen, C. Z. Chen, J. H. Gao, B. Zhou, and D. H. Xu, Phys. Rev. Lett. **124**, 036803 (2020).
34. R. Zhou, H. Lin, Y. J. Wu, Z. F. Li, Z. H. Yu, Y. Liu, and D. H. Xu, Photonics Res. **10**, 1244 (2022).
35. J. P. Jiang, B. Yan, Y. C. Peng, J. L. Xie, A. Q. Shi, and J. J. Liu, Opt. Lett. **47**, 437 (2022).
36. R. G. Gladstone, M. Jung, and G. Shvets, Phys. Rev. Lett. **128**, 026801 (2022).
37. L. He, W. X. Zhang, and X. D. Zhang, Opt. Express **27**, 25841 (2019).
38. Y. Q. Zeng, U. Chattopadhyay, B. F. Zhu, B. Qiang, J. H. Li, Y. H. Jin, L. H. Li, A. G. Davies, E. H. Linfield, B. L. Zhang, Y. D. Chong, and Q. J. Wang, Nature **578**, 246 (2020).
39. Y. Ota, F. Liu, R. Katsumi, K. Watanabe, K. Wakabayashi, Y. Arakawa, and S. Iwamoto, Optica **6**, 786 (2019).
40. C. Y. Ji, G. B. Liu, Y. Y. Zhang, B. S. Zou, and Y. G. Yao, Phys. Rev. A **99**, 043901 (2019).
41. A. Q. Shi, B. Yan, R. Ge, J. L. Xie, Y. C. Peng, H. Li, W. E. I. Sha, and J. J. Liu, Opt. Lett. **46**, 1089 (2021).
42. X. D. Chen, W. M. Deng, F. L. Shi, F. L. Zhao, M. Chen, and J. W. Dong, Phys. Rev. Lett. **122**, 233902 (2019).
43. X. F. Zang and C. Jiang, J. Phys. B-At. Mol. Opt. Phys. **43**, 065505 (2010).
44. L. J. Wang, L. Q. Yuan, X. F. Chen, and S. H. Fan, Phys. Rev. Appl. **14**, 014063 (2020).